A THEORY OF WAVE SCATTER FROM AN INHOMOGENEOUS MEDIUM WITH A SLIGHTLY ROUGH BOUNDARY AND ITS APPLICATION TO SEA ICE

Remote Sensing Laboratory
RSL Technical Report 177-53

S. K. Parashar
A. K. Fung
R. K. Moore

December, 1974

Supported by:

NATIONAL AERONAUTICS AND SPACE ADMINISTRATION
Lyndon B. Johnson Space Center
Houston, Texas 77058

CONTRACT NAS 9-10261

THE UNIVERSITY OF KANSAS CENTER FOR RESEARCH, INC.
2291 Irving Hill Drive—Campus West Lawrence, Kansas 66045

THE UNIVERSITY OF KANSAS SPACE TECHNOLOGY CENTER
Raymond Nichols Hall CENTER FOR RESEARCH, INC.
2291 Irving Hill Drive—Campus West Lawrence, Kansas 66045
Telephone:

A THEORY OF WAVE SCATTER FROM AN INHOMOGENEOUS MEDIUM WITH A SLIGHTLY ROUGH BOUNDARY AND ITS APPLICATION TO SEA ICE

Remote Sensing Laboratory

RSL Technical Report 177-53

S.K. Parashar
A.K. Fung
R. K. Moore

December, 1974

Supported by:

NATIONAL AERONAUTICS AND SPACE ADMINISTRATION
Lyndon B. Johnson Space Center
Houston, Texas 77058

CONTRACT NAS 9-10261

TABLE OF CONTENTS

	Page
ABSTRACT	i
1.0 INTRODUCTION	1
2.0 THEORY	1
3.0 COMPARISON OF THEORY AND EXPERIMENT	10
4.0 SUMMARY OF EXPERIMENTAL RESULTS	15
5.0 CONCLUSIONS	18
REFERENCES	22

ABSTRACT

An analytical theory of electromagnetic wave scattering from an inhomogeneous medium with a slightly rough boundary surface is formulated. The inhomogeneity in the medium is assumed to vary continuously in the vertical direction. In addition, it is also assumed to have a small random variation in the horizontal direction. The medium is assumed to consist of two layers. Maxwell's equations are solved by using the small perturbation method together with Fourier transform technique. The resulting differential equations are solved by using WKB and variation of parameter methods. Field amplitudes in each medium are determined by taking boundary conditions into account. The expressions for first order polarized radar backscatter cross-section σ^o are obtained.

An attempt is made to apply the developed theory to compute sea ice scatter. The complex permittivity of sea ice, which depends on both the temperature and salinity, varies with the depth of sea ice. In addition, there is certainly some variation in the horizontal direction. Thus, the developed model may be able to give useful estimates when applied to sea ice scattering. Numerical calculations are performed for polarized radar backscatter cross-section (σ_{VV}^o and σ_{HH}^o) at two frequencies, 13.3 GHz and 400 MHz. It can be shown that WKB method is applicable at both of these frequencies. These theoretical results are compared with the experimental results obtained from NASA Earth Resources Program mission 126. Theoretical results give the same absolute value of σ^o and the relative variation among the six ice types as is given by the experimental results.

1.0 INTRODUCTION

A theoretical model has been developed to describe the backscatter from sea ice. Computations based on this model agree well in principle but not always in detail with experimental observations performed in 1970 over the Arctic Ocean, north of Alaska. The theoretical model presented here takes into account small-scale roughness of the surface, average variation in dielectric properties with vertical position inside the ice, and horizontal small-scale inhomogeneities within the ice volume. Experimental observations with which the theory is compared were made by NASA Earth Resources Program aircraft in April, 1970, using scatterometers at 0.4 GHz and 13.3 GHz as well as an imaging radar at 16.5 GHz.

At the two higher frequencies, both theory and experiment indicate that the thinnest ice gives a moderate strength return. Ice of the next thickness category (in the neighborhood of 5 centimeters) gives the weakest return, and ice with increasing thickness results in increasing signal return. Both theory and experiment also show at 0.4 GHz that the thinnest ice gives the weakest return with the signal increasing as the ice thickness increases up to about 1 meter thickness and then decreasing for ice thicker than 1 meter.

This paper is a brief summary of some of the material contained in the doctoral dissertation at the University of Kansas by S. K. Parashar.*

2.0 THEORY

Ice on the polar seas is a complicated medium. The surface is exposed to blowing salt water and low air temperatures; the bottom is exposed to the sea. As the ice freezes, the salt water concentrates into brine and forms small pockets within the crystalline structure. Eventually, the pockets of brine also freeze if the temperature becomes low enough. Diffusion causes migration of the salt away from the surface toward the bottom of the ice; but some of the salt at the surface is replenished by the blowing sea-water spray. The amount of replenishment on the surface, the amount of freezing, the amount of snow cover and the rate of diffusion are all functions of the time of year and of the shorter-term weather variations.

---

*S. K. Parashar, Investigation of Radar Discrimination of Sea Ice, The University of Kansas, 1974, Ph.D. Dissertation. This material was also presented at the URSI Specialist Meeting held 23-26 September 1974 in Bern, Switzerland.

Because of the different temperature regimes at the surface and bottom of the ice, and because of the diffusion processes that take place, the dielectric properties of the ice vary with depth.

Because of the way in which the crystals are formed and of the way in which the brine concentrates in the ice, a vertically-oriented structure appears in cross-sections of the ice. Thus, one expects larger random inhomogeneities in the horizontal direction, but larger regular variation in the vertical direction. The surface of the ice is initially smooth but becomes rough because of fracturing, because of precipitation effects, because of the effects of spray hitting the surface and freezing irregularly, and because of the normal irregularity associated with the freezing of the brine. The surface effects due to the freezing precipitation and spray are relatively small scale; but some of the mechanical effects can be very large, as in the case of pressure ridges.

An additional phenomenon, which is ignored in the theoretical model developed here, is "rafting." This results when one sheet of ice is pushed beneath another due to wind and current in the sea. The result is discontinuity within the ice where the bottom of one sheet that formerly was in contact with the sea adjoins the top of the other sheet that formerly was in contact with the air. Because of the complexities associated with rafting, the theoretical model ignores these effects.

Figure 1 illustrates the fundamental theoretical model for this paper. Space is divided into three major regions: atmosphere, sea ice, and sea water, with the sea ice further subdivided into two other regions. Medium 1 is a region of decreasing permittivity, and medium 2 is a region of increasing permittivity with $z = z_1$ the boundary at the level of minimum permittivity. In this model the permittivity in the ice is assumed to consist of the sum of two components; of these, one is a function only of vertical position within the ice and the other is a function only of horizontal position. The vertically-varying component has a smooth variation and the horizontal variation is random. The surface of the ice adjacent to $z = z_0$ is considered rough, and the roughness at the bottom, $z = z_2$, is ignored. Of course, the bottom of thick sea ice is known to be very rough, but the signals are not expected to penetrate with enough strength that this roughness needs to be considered.

Figure 1 also illustrates that the incident angle is θ and the scattering angle with the vertical θ_s. The incident wave is in the XZ plane, but the scattered wave goes in a plane through the Z axis, making an angle ϕ_s with the X axis. Similar angles may be defined within the sea ice.

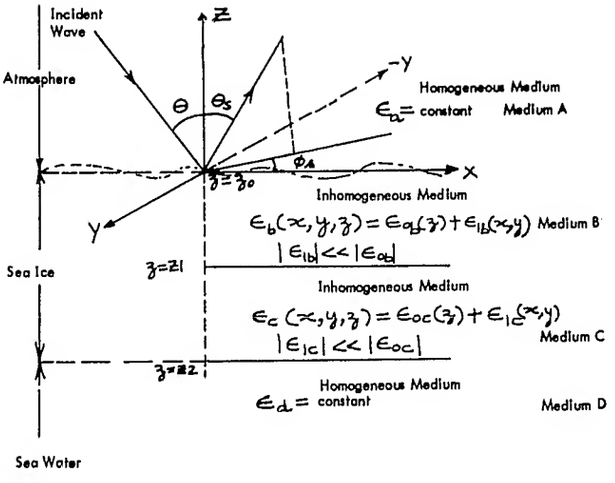

Figure 1. Theoretical Sea Ice Model.

In the analysis that follows, the profile within the ice of ϵ_{01} and ϵ_{02} is bi-linear; that is ϵ_{01} is a decreasing linear function and ϵ_{02} is an increasing linear function. The values at the top and bottom and at the central junction point, z, are based on temperature and salinity values for the type and thickness of ice being considered as reported by Hoekstra and Cappillino, 1971. Thus, the bi-linear profile is an approximation to the curvilinear profile actually measured by other investigators. No such profiles for the ice were measured at the time of the backscatter measurements.

Since no good information is available on the horizontal inhomogeneities either within the ice or at the surface, arbitrary selections of the parameters for these variations were made when the data were compared with the theory.

The waves in the homogeneous media air and sea satisfy the usual equations:

$$\nabla^2 E + K^2 E = 0 \tag{1}$$

$$K^2 = \omega^2 \mu \epsilon \tag{2}$$

In the inhomogeneous medium, a perturbation solution results in successive iterations. The wave equation to be solved is

$$\nabla^2 E' + k'^2(x,y,z) = -\nabla\left[\frac{\nabla \epsilon'(x,y,z) \cdot E'}{\epsilon'(x,y,z)}\right] \tag{3}$$

where k' is the wave number in the ice, E' is the electric field in the ice, and ϵ' is the permittivity in the ice. The value of k' is given by

$$k'^2(x,y,z) = k'^2_0(z) + \omega^2 \mu \epsilon'_1(x,y,z) \tag{4}$$

where k'_0 is the unperturbed value and $\epsilon_1'(x,y)$ is the randomly varying component associated with the first order solution. Thus the total field, after iterations, is

$$E = E_0 + E_1 + E_2 + \text{------} \tag{5}$$

Considering the equations for the zero order and first order solutions, we observe for the homogeneous medium that both orders of solution must satisfy the usual homogeneous wave equations.

$$\nabla^2 E_o + k^2 E_o = 0 \tag{6}$$

$$\nabla^2 E_1 + k^2 E_1 = 0 \tag{7}$$

Equation (8) shows the zero order form of the wave equation in the inhomogeneous ice medium, and (9) shows the equation for the first order solution in this medium. Clearly, (9) involves substitution of the solutions of (8) into the equation for E_1'.

$$\nabla^2 E_o' + k_o'^2(z) E_o' = -\nabla \frac{(\nabla \epsilon_o'(z) \cdot E_o')}{\epsilon_o'(z)} \tag{8}$$

$$\nabla^2 E_1' + k_o'^2(z) E_1' = -\frac{E_o' k^2 \epsilon_1'(x,y)}{\epsilon} + \nabla \frac{\left[\frac{\epsilon_1'(x,y)}{\epsilon_o'(z)} \nabla \epsilon_o'(z) \cdot E_o'\right]}{\epsilon_o'(z)} - \nabla \frac{[\nabla \epsilon_1'(x,y) \cdot E_o']}{\epsilon_o'(z)} - \nabla \frac{[\nabla \epsilon_o'(z) \cdot E_1']}{\epsilon_o'(z)} \tag{9}$$

The solutions of the equations in the atmosphere (6 and 7) are of course well-known. For horizontal polarization, they are

$$E_{xo} = E_{zo} = 0$$

$$E_{yo} = e^{-jkx\sin\theta}\left[e^{jkz\cos\theta} + V e^{-jkz\cos\theta}\right] \tag{10}$$

where V is the reflection coefficient.

In the homogeneous medium (atmosphere), we may write the solutions of equation (7) as a summation of plane waves in terms of their two-dimensional Fourier transforms A_x, A_y, and A_z, as shown in

$$E_{x_1}(x,y,z) = \frac{1}{2\pi} \iint_{-\infty}^{\infty} A_{x_1}(K_x,K_y)\, e^{j(K_x x + K_y y - K_z z)}\, dK_x dK_y \tag{11}$$

$$E_{y_1}(x,y,z) = \frac{1}{2\pi} \iint_{-\infty}^{\infty} A_{y_1}(K_x,K_y)\, e^{j(K_x x + K_y y - K_z z)}\, dK_x dK_y \tag{12}$$

$$E_{z_1}(x,y,z) = \frac{1}{2\pi} \iint_{-\infty}^{\infty} A_{z_1}(K_x,K_y)\, e^{j(K_x x + K_y y - K_z z)}\, dK_x dK_y \tag{13}$$

where

$$K_z = (K^2 - K_x^2 - K_y^2)^{1/2} \tag{14}$$

The zero order solution in the inhomogeneous medium can be obtained by solving the homogeneous wave equation

$$\nabla^2 E_o' + K_o'(z)\, E_o' = 0 \tag{15}$$

This results in

$$E_{x_o}' = E_{z_o}' = 0 \tag{16}$$

$$E'_{yo} = \frac{1}{\sqrt{K_1(z)}}\left[C_1 e^{j\int_{z'_o}^{z} K_1(z')\,dz'} + C_2 e^{-j\int_{z'_o}^{z} K_1(z')dz'}\right] e^{-jax} \tag{17}$$

where

$$K_1(z) = \left[K'^2_o(z) - a^2\right], \quad a = K\sin\theta \tag{18}$$

This solution was obtained by use of separation of variables, and the solution takes into account the vertical variation of k_o' by use of the WKB method.

The first order solution is obtained by solving an inhomogeneous wave equation for the Fourier transform of the field component.

$$\frac{d^2 F(K_x, K_y, z)}{dz^2} + K'^2_1(z) = S_z(K_x, K_y, z) \tag{19}$$

where S_z is the Fourier transform of

$$-\frac{\partial}{\partial z}\frac{\left[\frac{\partial \epsilon'_1(x,y)}{\partial y} E_{yo}\right]}{\epsilon'_o(z)}$$

This equation may be solved by methods similar to that used for solving the homogeneous equation (15) and variations of parameter methods (Boyce and Diprima, 1967), but, of course, the solution is much more complicated, as indicated by its form:

$$\begin{aligned} F(K_x, K_y, z) = \frac{1}{\sqrt{K'_1(z)}}\Bigg[& B_1(K_x, K_y)\, e^{j\int_{z'_o}^{z} K'_1(z')\,dz'} \\ & + B_2(K_x, K_y)\, e^{-j\int_{z'_o}^{z} K'_1(z')dz'} \\ & + \frac{1}{2j}\Bigg\{ e^{j\int_{z'_o}^{z} K'_1(z')dz'} \int_{z'_o}^{z} \frac{S_z(K_x, K_y, z')}{\sqrt{K'_1(z')}}\, e^{-j\int_{z'_o}^{z'} K'_1(t)dt}\, dz' \\ & - e^{-j\int_{z'_o}^{z} K'_1(z')\,dz'} \int_{z'_o}^{z} \frac{S_z(K_x, K_y, z')}{\sqrt{K'_1(z')}}\, e^{j\int_{z'_o}^{z'} K'_1(t)\,dt}\, dz' \Bigg\}\Bigg] \end{aligned} \tag{20}$$

Here,

$$K_1'(z) = \left[K_0'^2(z) - K_x^2 - K_y^2 \right] \tag{21}$$

To obtain the complete solution, the boundary conditions at the interfaces must be matched. The boundary conditions at the smooth interfaces are, of course, straight-forward. However, some discussion of the boundary conditions at the rough surface is in order. Since the interface between air and ice is rough, even horizontally polarized waves may have some Z component of the electric field in the reflected and transmitted values. Thus, the local slope of the small perturbations of the surface height z(x,y) must be considered. Hence, the boundary conditions that must be satisfied at this interface are

$$E_y - E_y' = -\frac{\partial z(x,y)}{\partial y}\left(E_z - E_z'\right) \tag{22}$$

$$E_x - E_x' = -\frac{\partial z(x,y)}{\partial x}\left(E_z - E_z'\right) \tag{23}$$

$$H_y - H_y' = -\frac{\partial z(x,y)}{\partial y}\left(H_z - H_z'\right) \tag{24}$$

$$H_x - H_x' = -\frac{\partial z(x,y)}{\partial x}\left(H_z - H_z'\right) \tag{25}$$

Here, we assume that the maximum value of z(x,y) is small enough so that

$$\int_0^{z(x,y)} K_0'(z')\,dz' \approx K_0'(0)\,z(x,y) \tag{26}$$

And, also, this means

$$K_0'[z(x,y)] \approx K_0'(0) \tag{27}$$

The total solution is very complicated and is not presented here in its entirety. Rather simply, the general form is given here. Equation (28) shows the form of the

horizontally polarized solution and

$$\sigma^{o}_{HH} = \langle |A_y(K\sin\theta, 0)|^2 \rangle 4\pi K^2\cos^2\theta \qquad (28)$$

The vertically polarized solution is of the form

$$\sigma^{o}_{VV} = \langle |-A_x(K\sin\theta,0)\cos\theta - A_z(K\sin\theta,0)\sin\theta|^2 \rangle \cdot \frac{4\pi K^2\cos^2\theta}{\eta} \qquad (29)$$

$$\sigma^{o}_{VH} = \sigma^{o}_{HV} = 0$$

Cross-polarized values of this differential scattering coefficient are zero in this solution.

The coefficients A_i are the Fourier transforms of the field solutions and because of the assumptions in obtaining the solution, they may be expressed as the sum of components due to surface roughness and due to horizontal inhomogeneities for the permittivity in medium 1 and medium 2. That is

$$A_i(K\sin\theta, 0) = M_0(M_1\bar{z} + M_2\bar{\epsilon}_2 + M_3\bar{\epsilon}_1) \qquad (30)$$

$\bar{z}$ = F.T. of $z(x,y)$; $\bar{\epsilon}_1$ = F.T. of $\epsilon_1(x,y)$;

$\bar{\epsilon}_2$ = F.T. of $\epsilon_2(x,y)$ (31)

Here the constants M_i include the effect of the smoothly varying permittivity change with depth in the ice. If we assume an exponential form for the correlation function,

the solutions of (28) (29) can be expressed in terms of the correlation lengths by

$$\sigma^{o}(K\sin\theta, o) = M_o M_o^* \left[\frac{L_s^2 \sigma_z^2 M_1 M_1^*}{(1+4L_s^2 \sin^2\theta)^{3/2}} \right.$$

$$\left. + \frac{L_{2v}^2 \sigma_{2v}^2 M_2 M_2^*}{(1+4L_{2v}^2 \sin^2\theta)^{3/2}} + \frac{L_{1v}^2 \sigma_{1v}^2 M_3 M_3^*}{(1+4L_{1v}^2 \sin^2\theta)^{3/2}} \right] \cdot \quad (32)$$

$$\cdot 4\pi K^2 \cos^2\theta$$

where L_s is a normalized surface correlation length in layer 1, and L_{2v} is a normalized volume correlation length in layer 2. The standard deviations for the respective media are given by σ_z, σ_{1v}, σ_{2v}, respectively.

This outline of the theory has only attempted to give an overview. The details require more space than is available for this paper. Nevertheless, the general concepts of the model, based on known variations of the permittivity with depth for different thicknesses and types of ice with random inhomogeneities in the volume and on the surface, give a solution of the form shown.

3.0 COMPARISON OF THEORY AND EXPERIMENT

The experiment was performed in April of 1970 directly north of Point Barrow, Alaska, over a region of the Arctic Ocean containing a wide variety of first-year and multi-year ice. The P-3 aircraft contained two scatterometers, one at 0.4 GHz made measurements with vertical, horizontal and cross polarizations. At 13.3 GHz, the scatterometer measured only vertical polarization returns. At 16.5 GHz, a side-looking radar was used to produce images with vertical, horizontal, and cross polarization.

The flight line was laid out as shown in Figure 2. The scatterometers were flown in parallel lines across an area viewed from four directions by the side-looking

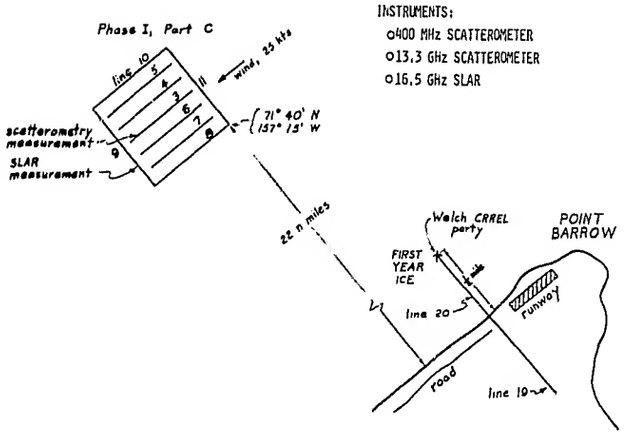
Phase I, Part C
line 10
wind, 25 kts
71° 40' N
157° 13' W
scatterometry measurement
SLAR measurement
22 n miles
Walch CRREL party
POINT BARROW
FIRST YEAR ICE
line 20
runway
road
line 10
INSTRUMENTS:
o400 MHz SCATTEROMETER
o13.3 GHz SCATTEROMETER
o16.5 GHz SLAR

Figure 2.

radar. That is, the side-looking radar images were produced by pointing the radar toward the inside of a square flight track, and all of the scatterometer lines were within this square.

The initial categories used in analysis of the scatterometer returns are listed in Table 1. Categorization of the ice observed by the scatterometer was achieved by interpretation of stereo photographs taken at the same time as the scatterometer data. The techniques for analyzing the photographs were shown to us by Mr. Vern Anderson, of the Photographic Interpretation Corporation, Hanover, New Hampshire.

Separation into one of the seven categories was achieved from the photographs. The assignment of thicknesses is based upon normal thicknesses for ice in such categories. No direct measurement was made of the ice thickness.

Categories 2, 3, and 4 all represent quite thin ice, since the maximum thickness of category 4 is only 30 cm. Categories 6 and 7, however, represent quite thick ice. In general, the boundary between ice too thin to be of significance to navigation and ice that will impede navigation is somewhere in the 5, 6, or 7 categories. On the other hand, even new ice can have a significant effect upon heat transfer between the water and the air.

Figure 3 shows the 13.3 GHz experimental results. At vertical incidence open water gives the maximum return, although at angles beyond about 20°, it might be confused with some other category; and at angles of 50 or 60 degrees, it gives one of the weakest returns. Category 7, multi-year ice, gives a stronger return than any other ice type at most angles of incidence. And category 6, the thick first-year ice, also clearly gives a strong return. Category 5 gives a fairly weak return. Figure 4 shows theoretical computations for the same frequency and ice conditions. The shapes of the curves are somewhat different from those of Figure 3. However, the order is almost the same at angles beyond about 25°. Absolute magnitudes predicted by the model are weaker at the larger angles than experiment shows. Perhaps a modification of the parameters for the surface roughness would result in a less steep slope and consequently larger signals at the large angles, like those observed experimentally. Nevertheless, the theoretical computations agree reasonably well in order with the experiments.

Figure 5 shows the corresponding theoretical calculations for horizontal polarization. The order of the categories is the same as observed experimentally with vertical polarization, but the slope of the horizontally polarized theoretical curves is muchsteeper than that of either the vertically polarized experimental or theoretical curves. Unfortunately, no experimental data were available for horizontal polarization to compare with this theory.

TABLE I.

CATEGORIES USED IN SCATTEROMETER

INITIAL ANALYSIS OF SEA ICE

CATEGORY	THICKNESS (CM)
1) Open Water	0
2) New Ice	0 - 5
3) Thin Young Ice	5 - 18
4) Thick Young Ice	18 - 30
5) Thin First Year Ice	30 - 90
6) Thick First Year Ice	90 - 180
7) Multi-Year Ice	180 - 360

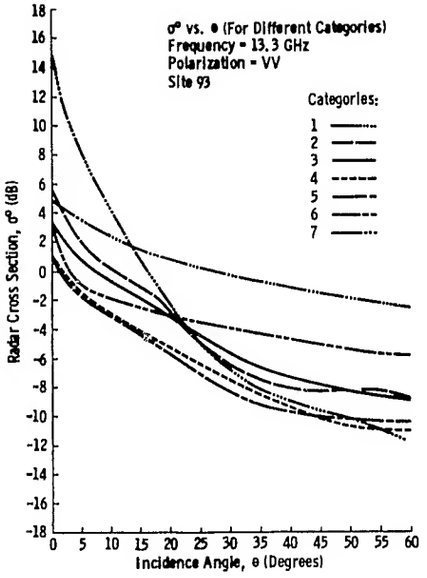

Figure 3. Experimental σ^{o} vs. θ for Different Categories, 13.3 GHz, VV.

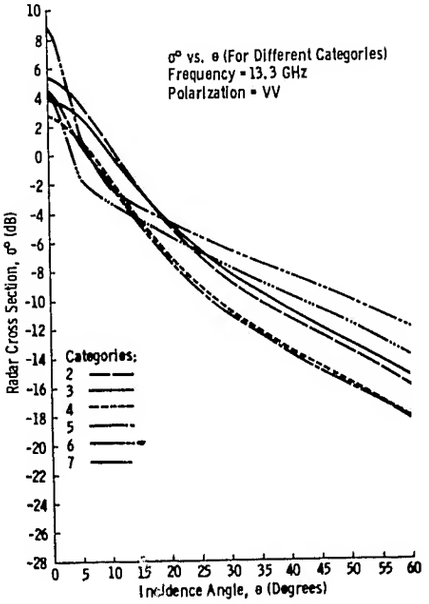

Figure 4. Theoretical σ^{o} vs. θ for Different Categories, 13.3 GHz, VV.

Figure 6 shows the experimental observations for vertical polarization at 400 MHz. Here the water is not as distinguishable from ice as it was at 13 GHz, and the difference between the different ice types is not clear. The strongest signals at large angles are from the moderate thicknesses of ice and the weakest are from the thin 5 to 18 cm. region. Note also that the absolute level of the scattering coefficient at large angles for this frequency is of the order of 20 dB lower than the absolute level at 13 GHz.

Figure 7 shows the theoretical calculations for the same frequency as Figure 6. The absolute level of the expected return is comparable with that observed. The relative sizes of the returns of the different categories at large angles is also about as observed. On the other hand, the shape of the curves for smaller angles does not seem to be the same as the observation. In general, however, the agreement is reasonably good between theory and experiment for this frequency and polarization.

Observations were made with other polarizations at 400 MHz, but the results are sufficiently similar to those for vertical polarization that they are not presented here.

4.0 SUMMARY OF EXPERIMENTAL RESULTS

A major purpose of theory and experiment on radar return from sea ice is determination of thickness. Thus, the best way to illustrate the usability of the scattering coefficient for thickness measurements is to plot scattering coefficient versus the best estimate we can make of the thickness. This has been done by using the mean thickness in each of the categories to represent that category, thus, obtaining one thickness value for each category. Figure 8 summarizes the results at 13.3 GHz with vertical polarization. Clearly, there is an ambiguity between new ice, category 2, and some of the thicker ice. However, if some other means can be used to establish the extent of the new ice, the remaining ice categories can be distinguished by the strength of the scattering. In fact, on an imaging radar, the texture of the pattern for new ice is quite different from that for the ambiguous thicker ice; so determination of ice thickness does appear feasible using this frequency and polarization.

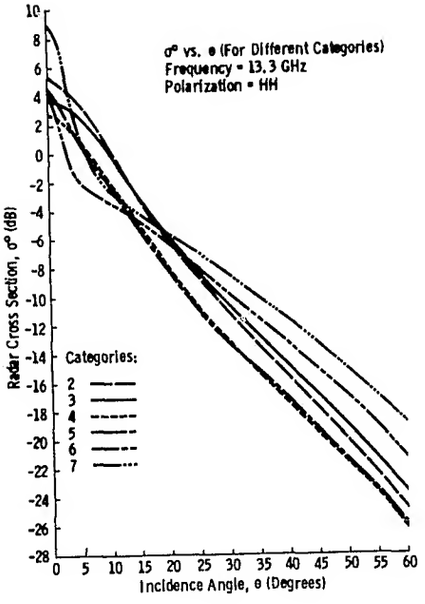

Figure 5. Theoretical σ° vs. θ for Different Categories, 13.3 GHz, HH.

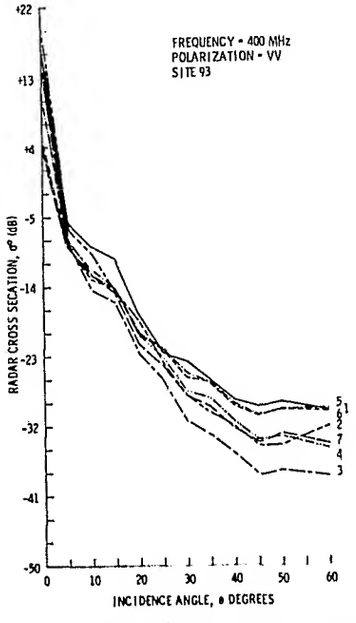

Figure 6. Experimental σ° vs. θ for Different Categories, 13.3 GHz, HH.

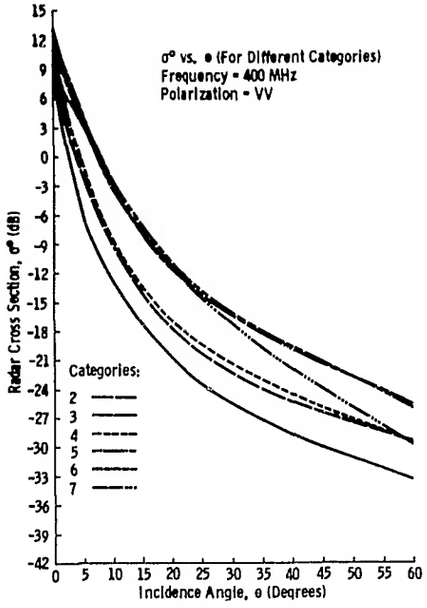

Figure 7. Theoretical σ^{o} vs. θ for Different Categories, 400 MHz, VV.

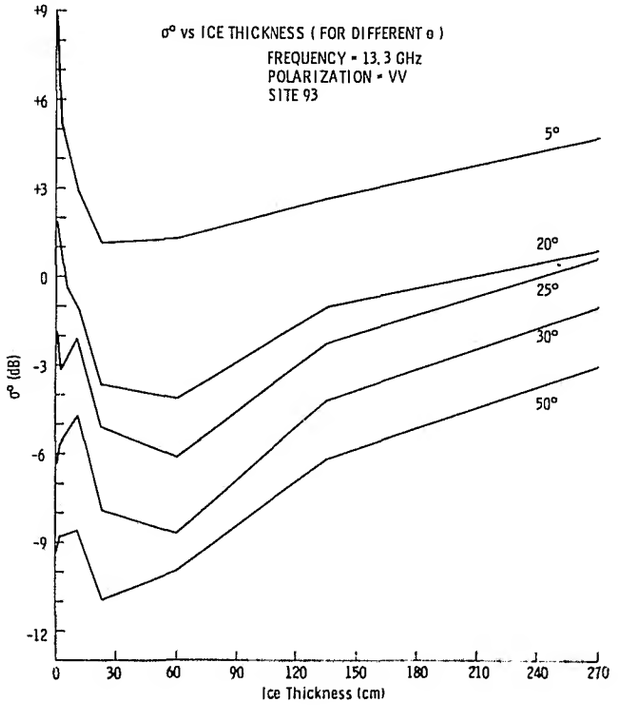

Figure 8.

The vertically polarized returns at 0.4 GHz are summarized in Figure 9. Note that category 2, which gave a moderately strong return for 13.3 GHz, here gives the weakest return. The strongest signals come from ice in the neighborhood of 1 meter thick, and older ice gives a weaker return. This was also the observation on the theory. Presumably, the difference in this property between 0.4 GHz and 13.3 GHz has to do with the relative degree of penetration of the ice in the two frequencies.

Figure 10 illustrates that the behavior of the cross-polarized return is similar to that of the like-polarized vertical return. Behavior for horizontal polarization is similar and is not reported.

Estimates were also made of the ability to distinguish ice categories on the 16.5 GHz imagery. Because the gray scale rendition of the images was not good, only three categories of ice plus the open water were used in the image analysis. That is, categories 2 and 3 were combined, categories 4 and 5 were combined, and categories 6 and 7 were combined. The resulting categories are shown in Table 2. With this type of categorization over 80 percent "correct" identification was achieved. With this good agreement between the radar result and the photo-interpretative categories, it is possible that a significant part of the disagreement occurs because of misclassification on the photographs rather than on the radar, although, of course, this cannot be quantitatively established. Figures 11 and 12 show images of the ice for the vertical and cross-polarized returns, with the different categories identified on the illustrations.

5.0 CONCLUSIONS

The theoretical model developed here gives results that coincide reasonably well in order of magnitude and in order of responses from the different types of ice. The theoretical responses calculated vary somewhat more rapidly with angle of incidence than do the experimental responses, with the difference being greater at 13.3 GHz than at 0.4 GHz.

The results of both experiment and theory indicate that the 13.3 and 16.5 GHz systems appear likely to be successful for measuring ice thickness. Presumably, the fact that there is moderate agreement between theory and experiment over the entire frequency range studied means that we can use the theory to interpolate for results at

TABLE II

CATEGORIES USED IN IMAGE AND LATER

SCATTEROMETER ANALYSIS OF SEA ICE

CATEGORY	THICKNESS (CM)
A) Open Water	0
B) Thin First-Year Ice	0 - 18
C) Thick First-Year Ice	18 - 90
D) Multi-Year Ice & Very Thick First-Year Ice	90 - 360

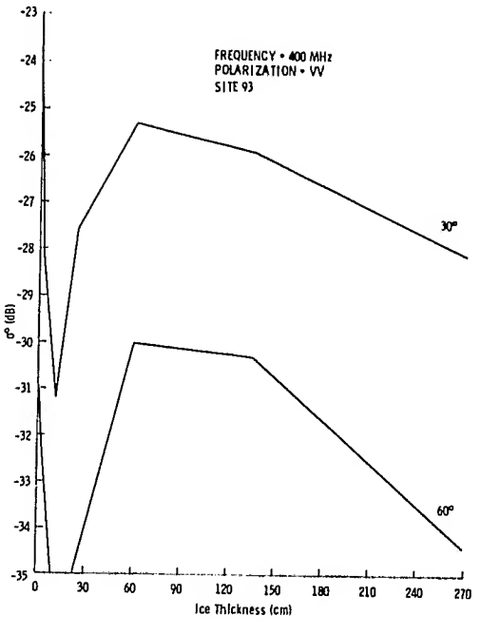

Figure 9. Experimental σ^{o} vs. Ice Thickness for Different θ, 400 MHz, VV.

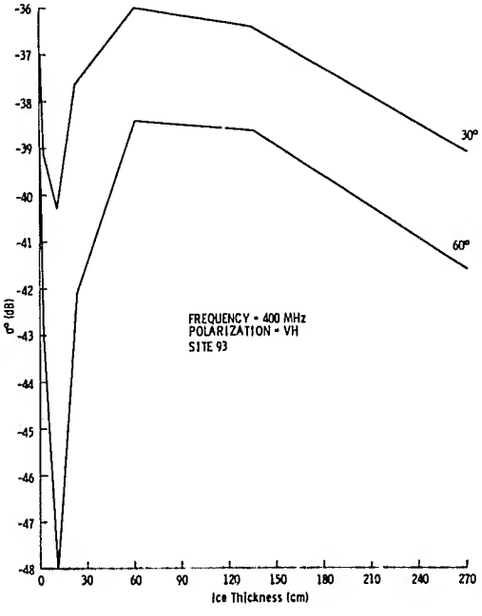

Figure 10. Experimental σ^{o} vs. Ice Thickness for Different θ, 400 MHz, VH.

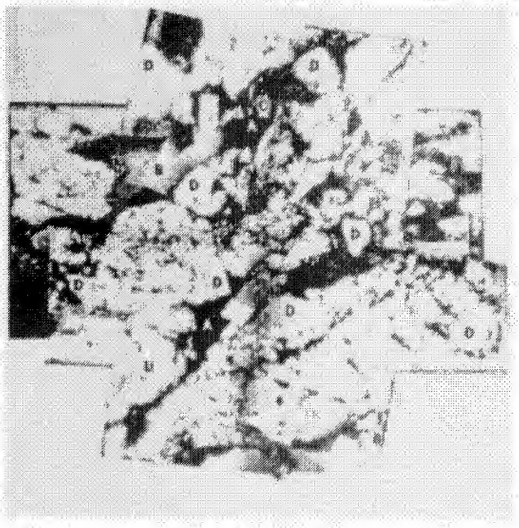

Figure 11. Mosaic of Radar Imagery, 16.5 GHz, VV, Real Aperture.

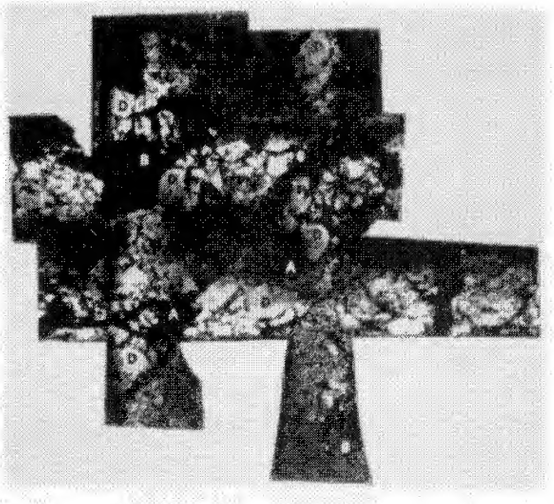

Figure 12. Mosaic of Radar Imagery, 16.5 GHz, VH, Real Aperture.

other frequencies. However, the frequency spacing is so wide that interpolation may not be very reliable because the size of the important random variations in different parts of the frequency range probably also differs.

REFERENCES

1. Hoekstra, P. and P. Cappillino, "Dielectric Properties of Sea Ice and Sodium Chloride Ice at UHF and Micro-Wave Frequencies," Journal of Geophysical Research, vol. 76, no. 20, pp. 4922-4931, July, 1971.

2. Boyce, W. E. and R. C. Diprima, Elementary Differential Equations and Boundary Value Problems, John Wiley and Sons, Inc., New York, May, 1967.